Debris expulsion as a rate determining process in fretting – the effect of slip amplitude on debris expulsion behaviour and rates

T Zhu, C.J. Bennett, P.H. Shipway

Faculty of Engineering, University of Nottingham, UK.

Abstract

In contrast to the well-established understanding of sliding wear, recent work has clearly demonstrated that the instantaneous wear rate in fretting of metals is dependent upon the contact size due to the fact that transport of species in and out of the contact are normally the rate-determining processes (RDPs), the processes being oxygen transport and debris transport respectively.

In this work, non-conforming (cylinder-on-flat) contacts were fretted with a range of slip amplitudes between ~ 5 µm and 80 µm, and the contact size-dependent wear coefficient was determined in each case. It was observed that although a slip amplitude threshold (below which wear does not proceed) may exist, this threshold is below the lowest slip amplitude examined in this work. However, as the slip amplitude was decreased, the number of cycles for wear to be initiated increased; for example, at the lowest slip amplitude examined in this work, measurable wear was not observed after 5 million fretting cycles but was observed after 10 million cycles.

The development of wear scar profile as a function of slip amplitude was also examined. It was observed that at a fixed number of cycles, smaller slip amplitudes resulted in W-shaped wear scars whereas larger slip amplitudes resulted in U-shaped scars. It was also observed that at a fixed slip amplitude, the scar shape developed from being U-shaped in the initial stages of fretting to W-shaped as the test proceeded. These changes in scar geometry are interpreted bearing in mind the fact that the scar size is also a function of changes in these parameters. Scanning electron microscopy was employed to aid understanding with the observations being interpreted in the framework of debris-ejection as the rate determining process. Reasons for the strong dependence of wear rate on slip amplitude are proposed.

1 Introduction

Fretting wear is a form of degradation that is commonly observed in a wide range of engineering applications due to system vibrations giving rise to relative motion between surfaces in contact. Fretting wear typically occurs at an interface in which oscillating tangential loads result in slip occurring across the interface, and where the amplitude of slip displacement (typically of the order of tens of micrometres) is generally small relative to the size of the contact (often termed a *closed contact*). The Archard wear equation was derived for sliding wear [1], and despite the significant difference between sliding and fretting wear with their open and closed contacts respectively, approaches based upon Archard's equation (here collectively termed *Archard-type approaches*) have been widely and successfully applied to fretting for a number of years [2, 3]. A literal application of an Archard-type approach indicates that the specific wear rate in fretting should be independent of a number of parameters where for many of which it is well known and understood that this is not the case, amongst these being slip amplitude, fretting frequency and contact size.

Despite the use of Archard-type approaches, key mechanistic differences between sliding and fretting wear have been well understood since the work of Godet [4] almost forty years ago. Here, it was argued that in fretting, the traditional definition of wear as the removal of material from surfaces is not sufficient to describe the amount of material lost due to wear; instead, a definition of wear needs to account for the flows of debris out of the contact and should instead be defined as the amount of material ejected from the contact. Understanding of the fretting wear process needs to focus upon debris formation and ejection as indicated by the third body approach [4] and also upon the concept of tribology circuit [5], rather than considering material removal only as suggested by the Archard wear equation [1]. Although this understanding has been widely accepted for a number of decades, only recently has a model for the role of contact size on the rate of debris flow out of the contact been developed [6].

Whilst Godet and co-workers first clearly outlined the importance of removal of debris from the contact in fretting wear, Fouvry and co-workers were the first to clearly outline the role of oxygen transport into the contact in fretting [7, 8]. In fretting wear of metals, the debris that is expelled from the contact is typically very largely comprised of metal oxides [9] and given that this oxide is formed throughout the fretting contact, oxygen transport into all areas of the contact is therefore critical to the continual process of fretting wear. Fouvry and co-workers first suggested that under certain fretting conditions, the rate of oxygen transport into the interface may not be sufficient to replenish oxygen consumed in the fretting process [8] and subsequently went on to develop a "contact oxygenation description of fretting" [10] which provided a framework for interpreting the effects of fretting parameters on wear rates and mechanisms in terms of their effect on oxygen concentration in the contact; more recently, this has been further developed into their advection-dispersion-reaction (ADR) model for use in fretting [11].

More recently, Shipway and co-workers have brought together the understanding of these key physical processes in their rate-determining process (RDP) model of fretting [12] where they proposed that there are three key processes in fretting wear of metals as follows: (i) oxygen transport into the contact; (ii) formation of oxide-based wear debris in the contact and (iii) ejection of this wear debris from the contact. They argued that to maintain system equilibrium in steady-state fretting, the three processes must operate at the same rate as each other (i.e. that debris cannot be ejected from the contact faster than it is formed, and debris cannot be formed faster than it is ejected) and that accordingly, the actual wear rate observed is the rate of the process with the lowest rate of the three processes, with this process being termed the RDP. To illustrate the framework, they proposed simple, physically-based processes for each of the three processes which then allowed an understanding of the effect of fretting parameters (such as slip amplitude, fretting frequency, contact size etc) upon the observed rate of wear to be understood. In the abstract to their paper [12], they stated:

> *"A number of assumptions have been made in deriving the equations which describe the key processes and it is recognised that these equations themselves may be refined in light of future research; however, any such revised equations can simply replace those proposed as part of the rate-determining process framework."*

To illustrate the RDP approach , a number of assumptions were made about the rates of the various processes, and amongst these were the assumptions that the maximum volume of debris expelled from the contact per cycle $\left(\frac{dV}{d\mathrm{N}}\right)$ is (i) directly proportional to the slip amplitude, δ^* and (ii) directly

proportional to the contact pressure , p. The outcome of making these assumptions is that it is predicted that the maximum wear rate which can be sustained (under conditions where debris ejection from the contact is the RDP) is independent of the slip amplitude, δ^*. There are papers in the literature (including one by Shipway and co-workers which we consider to be erroneous [13]) which are in accord with this position; however, this position is clearly not in accord with the general and widely-held understanding of the role of slip amplitude in fretting as articulated by Vingsbo and Söderberg [14] as illustrated in Figure 1, where it is indicated that in the gross sliding fretting regime, the specific wear rate increases by approximately two orders of magnitude as the far-field displacement amplitude (distinct from the slip amplitude) is increased from about 30 μm to 300 μm before entering the regime of reciprocating sliding wear.

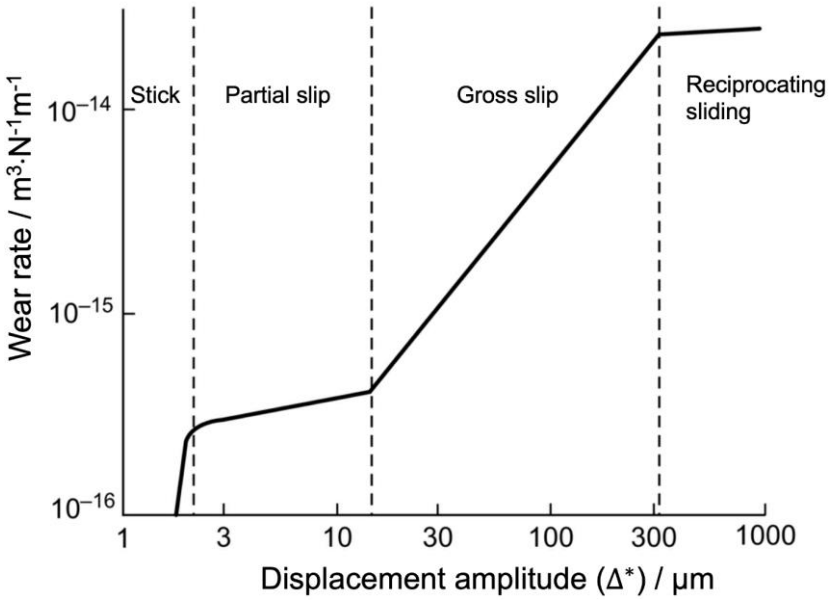

Figure 1 Illustration of the change of specific wear rate with the increase of the displacement amplitude in fretting (from [15] after [14]).

To fully understand the role of slip amplitude in fretting, its effects on both debris formation and debris ejection must be discussed separately, which requires studies to understand the underlying mechanisms and RDPs so that a coherent physical model can be established. It has been generally accepted that an increased slip amplitude can enhance the rate of debris ejection [16, 17]. However, a change in the slip amplitude (with all other parameters remaining constant) also results in a change in the power dissipated in the contact and will result in a change in the time-based rate of wear (as opposed to the exposure-based rate of wear) [18]. It may also affect the rate of debris formation through a change in the balance between the time-based rate of oxygen supply and the time-based rate of debris formation [19, 20]. A change in the slip amplitude will also affect the local temperature as the power dissipated into the contact as the slip amplitude changes, with this potentially influencing both the rate of debris formation and the rate of debris ejection from the contact [9, 21, 22].

The effect of slip amplitude on debris ejection is better understood compared to its impact on debris formation. Heredia and Fouvry [23] argued that there is a threshold of slip amplitude, below which the wear process seems to cease to occur; it was postulated that a sufficient slip amplitude is required to initiate the wear process in fretting, allowing debris to be ejected from the contact, thereby

promoting continuous wear. Fouvry et al. [17] also proposed that a larger slip amplitude can enhance the rate of debris ejection and argued that, when a larger slip amplitude is employed, debris can be ejected faster and thus a greater proportion of the energy dissipated within the contact can contribute to debris formation. A similar view was proposed by Aldham et al. [16] and Warburton [24] who suggested that larger slip amplitude tends to create a rougher contacting surface and gives wear particles a higher velocity, and hence the oxide debris can be transported more efficiently away from the site of its generation.

One of the consequences of an increased rate of debris ejection is that the formation of protective debris beds is reduced. It has been found that wear scars formed with a larger slip amplitude exhibit a significantly higher degree adhesive damage than those with smaller slip amplitudes [16, 24, 25], although it may be argued that this is due to oxygen starvation as oxygen transport becomes the RDP [12]. In work investigating the role of temperature in forming glaze layers in fretting contacts (where the wear rate drops to almost zero), it was found that the temperature at which a glaze layer was formed first was elevated by an increase in slip amplitude; it was argued that the larger slip amplitude resulted in a higher rate of debris expulsion, thus reducing its residence time in the contact and thus limiting its tendency to sinter into a coherent and protective debris bed [26].

As observed by Fouvry et al. [19], the slip amplitude also exerts an influence upon the shape of the fretting wear scar. It was found that there seems to exist a transition from W-shaped wear scar (where the apparent depth of wear is a maximum near the edge of the scar and reduces towards the centre) to a U-shaped scar (the wear is at its maximum at the centre of scar and reduces monotonically towards the edge) with an increase in slip amplitude. The nature of the material at the centre of a W-shaped scar has been the subject of debate: it could be either a build-up of oxide debris at the centre of a U-shaped metal surface [19, 27], or it could be a metallic central region dominated by adhesive damage surrounded by a more worn region associated with the formation of oxide debris [10, 28, 29]. Whilst the nature of W-shaped wear scars is not always characterized (and indeed may differ in different situations), the occurrence of a U-shaped scar is normally associated the higher rate of debris ejection.

A previous paper by Zhu et al. [6] addressed fretting wear of a long contact (where debris escape from the contact occurred only parallel to the direction of fretting motion); a governing equation was proposed linking the instantaneous wear rate, $\frac{dV_w}{dE_d}$, with the width of the wear scar, x, as follows:

$$\frac{dV_w}{dE_d} = \frac{k}{x} \tag{1}$$

The parameter k in Equation 1 acts as single parameter characterising the instantaneous wear rate for tests under certain conditions. Whilst this equation has general applicability for contacts where debris ejection is the RDP [12], the concept was further developed [2] to a produce a general form of wear equation which states that, for a variety of commonly-employed non-conforming test-piece configurations (such as sphere-on-flat, cylinder-on-flat, and crossed-cylinders) the wear volume, V_w, can be related to the energy dissipated during the test, E_d^n, as follows:

$$V_w = KR^{n-1}E_d^n \tag{2}$$

where R is the radius of any non-plane member of the specimen pair and K is a constant. The development of the RDP concept of fretting wear [12] is built upon an understanding of the key physical processes which govern fretting wear into a coherent framework. However, it is recognised that to fully realise the potential of such a model, the influence of various test parameters on the underpinning equations for oxygen transport into the contact, debris formation in the contact and debris ejection from the contact need to be understood. In this work, the role of slip amplitude on the fretting wear of a self-mated steel cylinder-on-flat contact is explored in terms of initiation of wear, wear rates and debris retention and removal from the contact. To ensure that steady state conditions are reached, test durations longer than those commonly reported in the literature are employed.

2 Experimental methods

2.1 Materials and test procedures

All of the specimens used in this work were produced from a high strength alloy steel (BS S132), the composition of which is presented in Table 1 with the specimen blanks being subjected to a commercially relevant heat treatment cycle, the details of which can be found elsewhere [30]. The specimens were subsequently ground into flat and cylindrical specimens as shown in Figure 2. All of the specimens had a width of 10 mm, while the cylindrical specimens were manufactured with a radius of 6 mm.

Table 1: Chemical composition of the high strength steel (wt.%) [30]

C	Mo	V	Cr	Si
0.35-0.43	0.8-1.10	0.15-0.25	3.0–3.5	0.1-0.35
Mn	Ni	P	S	Fe
0.4-0.7	<0.3	<0.007	<0.002	Balance

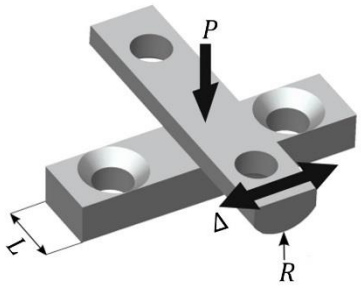

Figure 2 Illustration of the cylinder-on-flat specimen configuration applied in fretting tests: L is the length of the line contact, 10 mm; R is the radius of the cylindrical specimens, namely 6 mm; P is the normal load, 450 N; Δ^* is the applied displacement.

The pre-test preparation work involved thorough demagnetisation of the specimens and surface degreasing, before they were rinsed with industrial methylated spirit (IMS) and dried. Specimens were arranged in a cylinder-on-flat configuration for the fretting tests (Figure 2) producing an initial

line contact with a length of 10 mm. The flat specimen was mounted on a stationary lower specimen mounting block (LSMB) and the cylindrical specimen was attached to a moving upper specimen mounting block (USMB). A constant normal load, P, was applied to the USMB through a dead weight. An oscillatory motion with an applied displacement, Δ (with Δ^* referring to the applied displacement amplitude), was generated by an electromagnetic vibrator (EMV) and applied to the USMB. Throughout the test, the relative displacement (Δ) between the USMB and LSMB was monitored using a capacitance displacement sensor; the tangential traction force across the specimen pair contact, Q (with amplitude Q^*), was measured by a piezoelectric load cell. Both the tangential traction force and the relative displacement were sampled at a rate of 200 measurements for each fretting cycle. These data were used to plot fretting loops, with these being used to aid deconvolution of elastic deformation (system compliance) and slip in the fretting cycles [13]; a schematic diagram of a fretting loop is presented in Figure 3 where the key parameters of the displacement amplitude, Δ^*, the slip amplitude, δ^*, and the energy dissipated per cycle, E_d, are illustrated. In these tests, displacement amplitude, Δ^*, is the test control parameter, whilst the slip amplitude, δ^*, is a quantity derived following a test. In addition, the energy dissipated during a single fretting loop, E_d, can be derived post-test from the area enclosed by the fretting loop based on methods proposed by Fouvry et al. [27, 31]; the accumulated dissipated energy through a test is simply the sum of E_d from the individual loops.

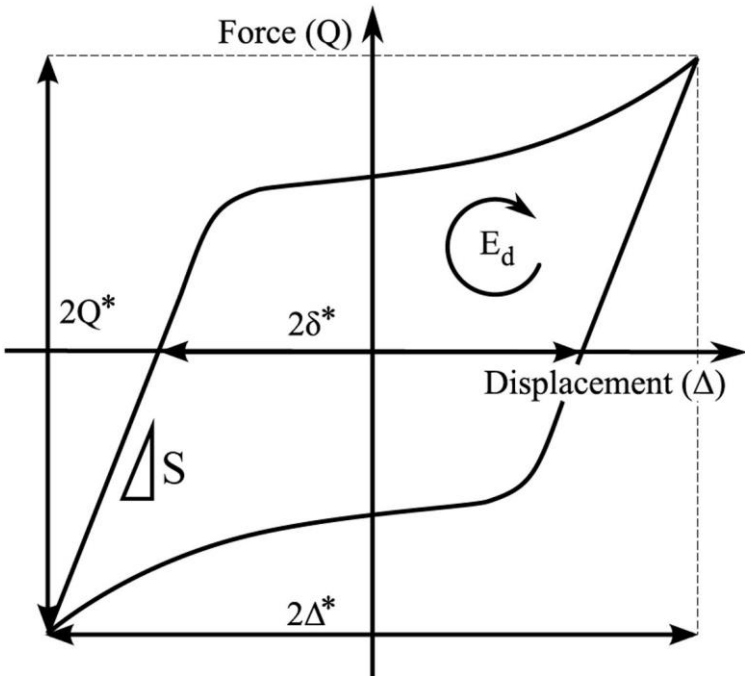

Figure 3 Schematic diagram of a fretting loop showing the relationship between the displacement amplitude, Δ^*, and the local contact slip amplitude, δ^* [32].

The energy-based coefficient of friction (ECoF), μ_e, can be calculated as follows:

$$\mu_e = \frac{E_d}{4\,\delta^*\,P} \tag{3}$$

All tests were conducted at ambient temperature with the same normal load, P, and frequency, f, over a range of test durations from 1 × 10^6 cycles to 10 × 10^6 cycles. Test conditions are summarised in Table 2.

Table 2: Summary of the fretting test conditions.

Normal load (P) / N	450
Displacement amplitude (Δ^*) / µm	10, 15, 20, 25, 50, 100
Cylindrical specimen radius (R) / mm	6
Test duration (N) / 10^6 cycles	1, 5, 10
Frequency (f) / Hz	20
Temperature (T) / °C	Ambient temperature

2.2 Characterization of wear scars and debris

Following a fretting test, the wear volume and the wear scar surface topography of specimens were evaluated via profilometry, whilst the nature of the wear scar and the distribution of wear debris were characterised using scanning electron microscopy (SEM). The worn specimens were ultrasonically cleaned in a bath of IMS to remove any debris not adhered to the worn surfaces, whereupon profilometry was then conducted using an Alicona G5 profilometer to determine the volume of material removed due to wear and assess the worn profiles of the wear scars. Average profiles across scars were generated by taking the average of individual profiles across the full scar width.

SEM was used to characterise the wear scar and the distribution of the oxide debris using a Philips XL30 microscope. Images were taken using both secondary electron (SE) and backscattered electron (BSE) imaging techniques, with BSE imaging being particularly useful since it allows oxide debris (with its lower average atomic number) to be readily distinguished from the metallic substrate as a result of its lower imaging brightness. Images were taken of scars both in plan view and in cross-section, the section being made such that the direction of fretting motion lies in the plane of the cross-section.

3 Experimental results

3.1 Fretting loops and their analysis

Examination of experimental data shows that in the early stages of the test, fretting loops were unsteady, but steady state was quickly achieved with the loops remaining stable throughout the rest of test. As an example to illustrate the stability of the loops, averaged fretting loops over the first 10%, the mid 10% and the last 10% of a test conducted with Δ^* = 25 µm and N = 5×10^6 cycles were produced and are presented in Figure 4a. Averaged fretting loops were subsequently calculated over the last 10% of tests and examples such averaged loops from tests with durations of N = 5×10^6 cycles and with a range of displacement amplitudes from Δ^* = 10 µm to Δ^* = 50 µm are presented in

Figure 4b. Within each loop, it can be seen that after the period of elastic deformation associated with induced by the compliance of system, the tangential force (Q) continues to increase during the relative motion (slip) between the first bodies. The system stiffness S (i.e. the gradient of the elastic part of the fretting loops as illustrated in Figure 3) was calculated to be 33 ± 3 N·μm^{-1}. It should be noted that the maximum tangential forces exhibited in tests conducted with Δ^* = 10 μm and Δ^* = 15 μm are similar to each other, but significantly lower than those observed in the tests conducted with larger displacement amplitudes. Experimental data from tests conducted with Δ^* = 100 μm are also used in the current study, but the maximum duration of these tests was N = 1×10^6 cycles; it is noted here that their fretting loops exhibit a system stiffness within the range identified for the loops presented in Figure 4 along with a similar maximum tangential force (Q^*). A characteristic tangential force for the loop is often presented in the form of μ_e, and the dependence of μ_e with Δ^* (and therefore with δ^*) will be presented later (Figure 6).

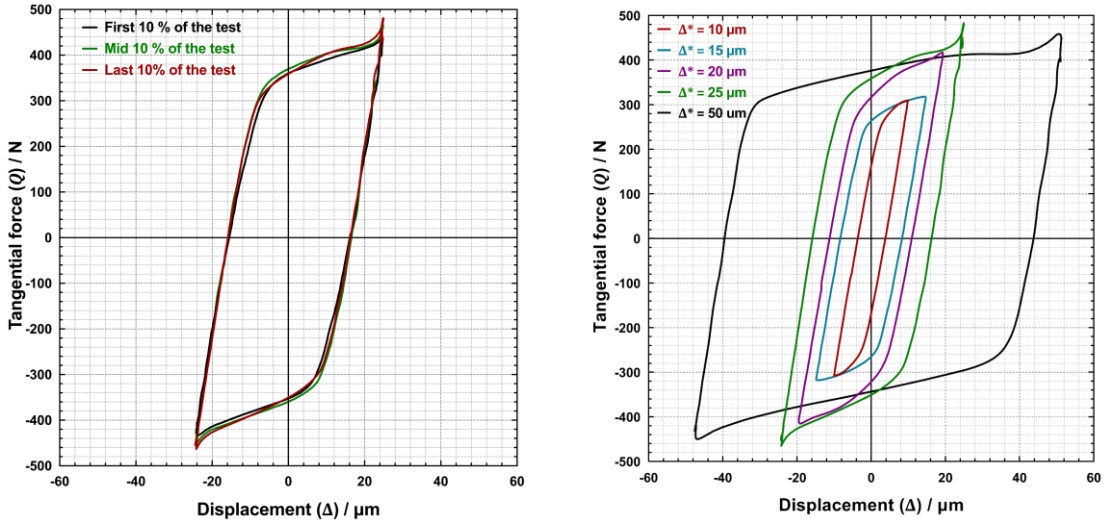

(a) (b)

Figure 4 Plot of averaged fretting loops for tests: (a) from the first 10%, the mid 10% and the last 10% of the test conducted with Δ^* = 25 μm and N = 5×10^6 cycles; (b). with varying displacement amplitudes from Δ^* = 10 to 50 μm for N = 5×10^6 cycles with the loops shown being average loops over the last 10% of each test.

Distinguishing slip amplitude (δ^*) from displacement amplitude (Δ^*) is important as the former represents the actual slip occurring between first bodies, and it can be calculated from the fretting loops by removing the elastic displacements from the loop. The slip amplitude in each cycle of a test, $\delta^*(i)$, was evaluated, and from this a single quantity to characterise the slip amplitude for the whole test (δ^*) was determined as the average of $\delta^*(i)$. In the current study, for tests with different displacement amplitudes, varying from Δ^* = 10 μm to Δ^* = 100 μm, their corresponding slip amplitudes across different test durations are relatively steady. The statistical analysis of slip amplitudes shows that variations of δ^* for each Δ^* at different number of cycles are small, with the RSD (relative standard deviation, defined as the ratio of one standard deviation to the mean) ranging from a minimum of 0.5% for Δ^* = 20 μm to a maximum of ~21% for Δ^* = 10 μm. The average values and variation of δ^* across different test durations for each Δ^* are presented in Table 3. The following

analysis to understand the dependence of wear rate upon displacement amplitude (therefore, the slip amplitude) will be based on the average value of slip amplitude, δ^*.

Table 3 Summary of the change of δ^* with the corresponding evolution of μ_e and k as Δ^* increases.

Δ^* / μm	δ^* / μm	μ_e	k / mm^4·kJ^{-1}
10	5.36 ± 1.12	0.61 ± 0.01	0.0004
15	8.12 ± 0.27	0.67 ± 0.04	0.0034
20	11.54 ± 0.06	0.78 ± 0.01	0.0123
25	15.91 ± 1.85	0.80 ± 0.02	0.0248
50	41.14 ± 0.46	0.79 ± 0.01	0.0375
100	82.08 ± 0.58	0.79 ± 0.01	0.0521

3.2 Coefficient of friction

Figure 5 is a plot of evolution of ECoF ($\mu_e(i)$) over a test of duration of N = 5×10^6 cycles for two displacement amplitudes, namely Δ^* = 10 μm and Δ^* = 50 μm. As can be seen, the evolution of $\mu_e(i)$ throughout the test is similar for both displacement amplitudes. The increase of $\mu_e(i)$ is rapid at the beginning of the test, followed by a rapid reduction to a relatively steady value which is characterised by small fluctuations around that steady value. Therefore, similar to the analysis of fretting loops in Figure 4, the averaged value of ECoF over the last 10% of the test duration was calculated to represent μ_e for each individual test.

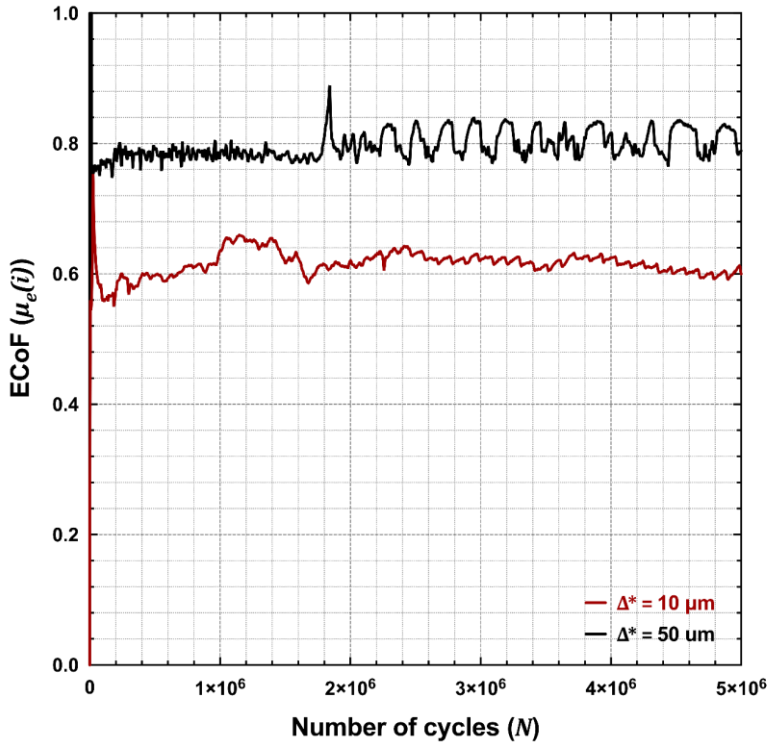

Figure 5 **Plot of evolution of ECoF ($\mu_e(i)$) over a test of N = 5×10^6 cycles for two displacement amplitudes, namely Δ* = 10 and Δ* = 50 µm.**

The average values of ECoF (μ_e) calculated from each test in the current study are plotted against the corresponding slip amplitude (δ^*) in Figure 6, with the error bars indicating the standard deviation of μ_e for each test. As can be seen, values of μ_e across different test durations for each slip amplitude are reasonably stable. It can be seen that μ_e increased rapidly from a value around 0.6 to around 0.8 as the slip amplitude, δ^*, was increased from ~5 µm to ~15 µm and then remained stable at around 0.8 as the slip amplitude was further increased. Averaged ECoF across different test durations can be determined, the values of which are summarised in Table 3.

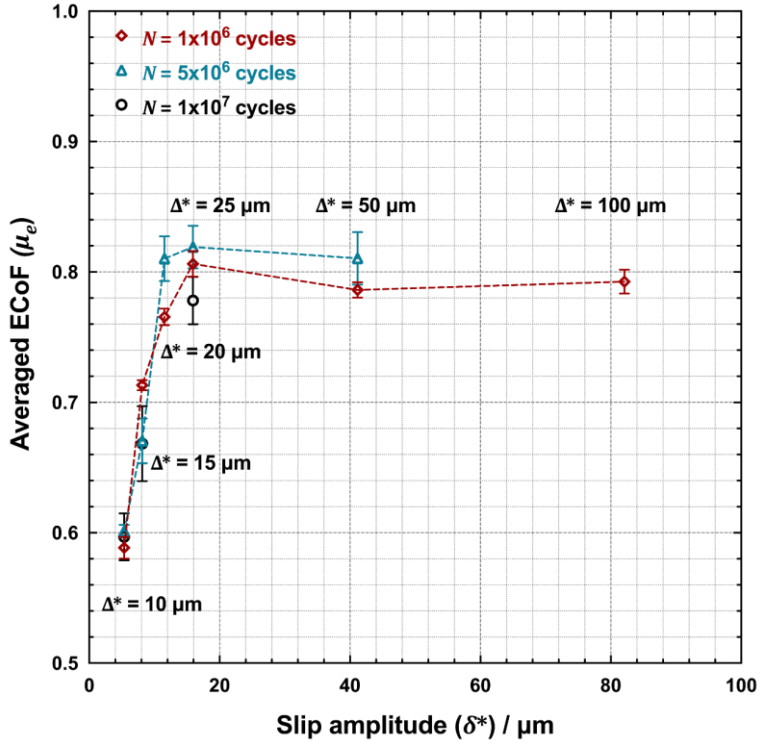

Figure 6 **Plot of averaged ECoF against slip amplitude for tests of varying duration (N = 1x10^6 cycles, 5x10^6 cycles and 1x10^7 cycles); values of ECoF were taken as the average of the last 10% of test duration.**

3.3 Wear scar analysis – scar profiles

Figure 7 shows the averaged profile of wear scars on flat specimens for tests conducted with varying displacement amplitude, from Δ* = 10 µm to Δ* = 50 µm for both N = 1×10^6 cycles and for N = 5×10^6 cycles. It can be seen that all wear scars developed as expected in both depth and width with the increase of test duration, except for tests conducted with Δ* = 10 µm. For Δ* = 10 µm, no clear evidence of the evolution of wear scar in terms depth or width was observed at least until N = 5×10^6 cycles.

A U-shaped wear profile is clearly developed for tests with Δ* = 50 µm. As demonstrated in previous work [6], this general wear scar shape is formed very early in the test (in this previous work, it was observed as early as N = 5×10^3 cycles). In contrast, for the tests conducted with displacement amplitudes within the range from Δ* = 15 µm to Δ* = 25 µm, the wear scar starts to show the early

sign of forming a W-shape by N = 1×10^6 cycles, with a W-shape wear scar being fully developed by N = 5×10^6 cycles. For example, the wear scar of the test conducted at Δ* = 25 μm seems to be at the edge of the transition from U-shape to W-shape after N = 1×10^6 cycles, and appears to exhibit features from both shapes; however, when the test duration was extended to N = 5×10^6 cycles, it can be seen that the W-shape of the wear scar has more fully developed.

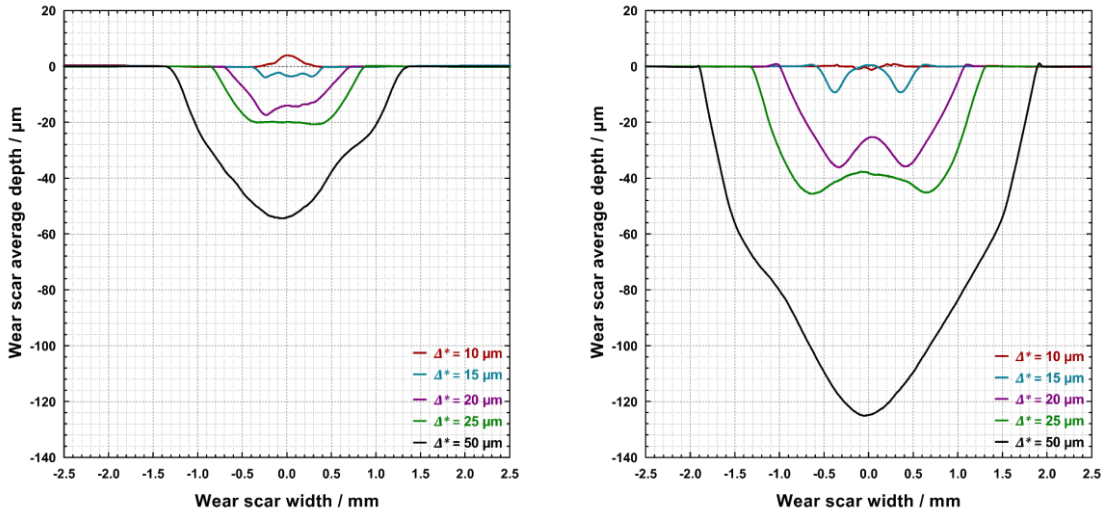

Figure 7 Averaged profiles of fretting wear scar on flat specimens for fretting tests at varying displacement amplitudes, from Δ* = 10 μm to Δ* = 50 μm. Experiments were conducted with (a) 1×10^6 cycles (b) 5×10^6 cycles.

To further investigate the development of W-shaped scars, some further extended tests with N = 10×10^6 cycles were carried out, and the average profiles of their corresponding wear scars are presented in Figure 8. As can be seen, for tests conducted with Δ* = 25 μm, the wear scar at N = 10×10^6 cycles clearly exhibits a properly formed W-shape. The fully developed W-shaped wear scar for tests with Δ* = 15 μm at N = 5×10^6 cycles is more developed as the tests duration is extended to 10×10^6 cycles. The wear scars for tests with Δ* = 10 μm exhibit the most dramatic change when the test duration was elongated to N = 10×10^6 cycles: the wear scar exhibits very little wear after N = 5×10^6 cycles but forms a clear W-shape after N = 10×10^6 cycles.

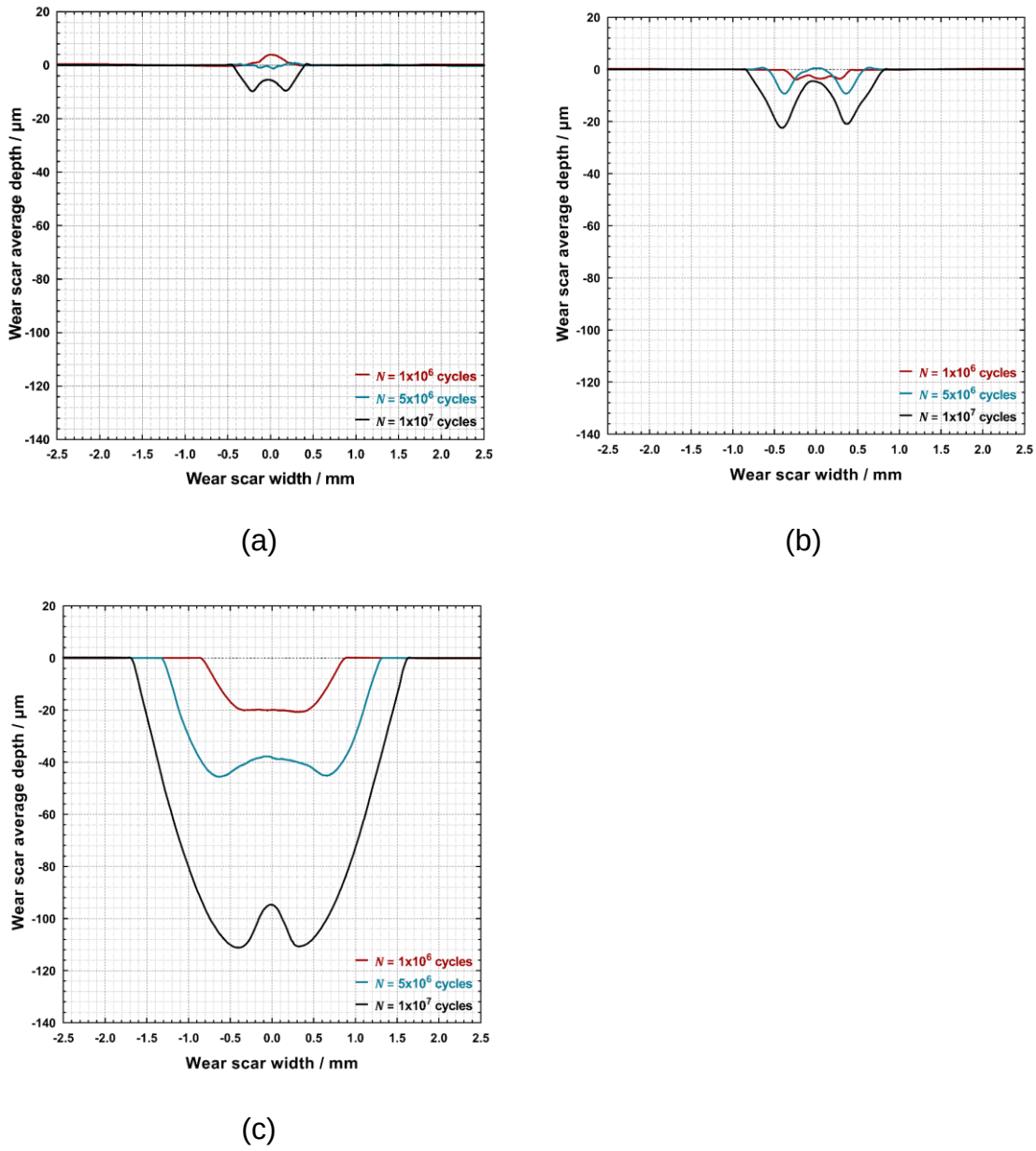

Figure 8 **Evolution of averaged profiles of fretting wear scar on flat specimens as a function of test duration (1, 5 and 10×10^6 cycles) for three different applied displacement amplitudes; (a) Δ^* = 10 µm; (b) Δ^* = 15 µm; (c) Δ^* = 25 µm.**

3.4 Wear scar analysis – debris type and distribution

Plan view BSE micrographs of the flat specimens for a range of displacement amplitudes for two fretting test durations (1×10^6 cycles and 5×10^6 cycles) are presented in Figure 9. A relationship between the displacement amplitude (and thus the slip amplitude) and the debris retention within the contact can be observed. It clearly shows that as the displacement amplitude is increased, the wear scar size is increased but the oxide debris is more sparsely distributed across the wear scar leaving the underlying metallic material more exposed. For tests conducted at Δ^* = 10 µm, the existence of a compact oxide bed across the wear scar can be observed. Such an oxide bed is still present for the tests conducted with Δ^* = 15 µm, except that it only exists at the centre of wear scar, while the metallic surface is more prominent towards the edge of wear scar. This trend of the oxide bed being

unevenly distributed across the wear scar is continued and amplified for tests conducted with higher displacement amplitudes. The BSE images of the wear scar following fretting with $\Delta^* = 50$ µm also indicate the possibility that a coherent oxide bed may form within the wear scar which then delaminates due to the relative motion between first bodies.

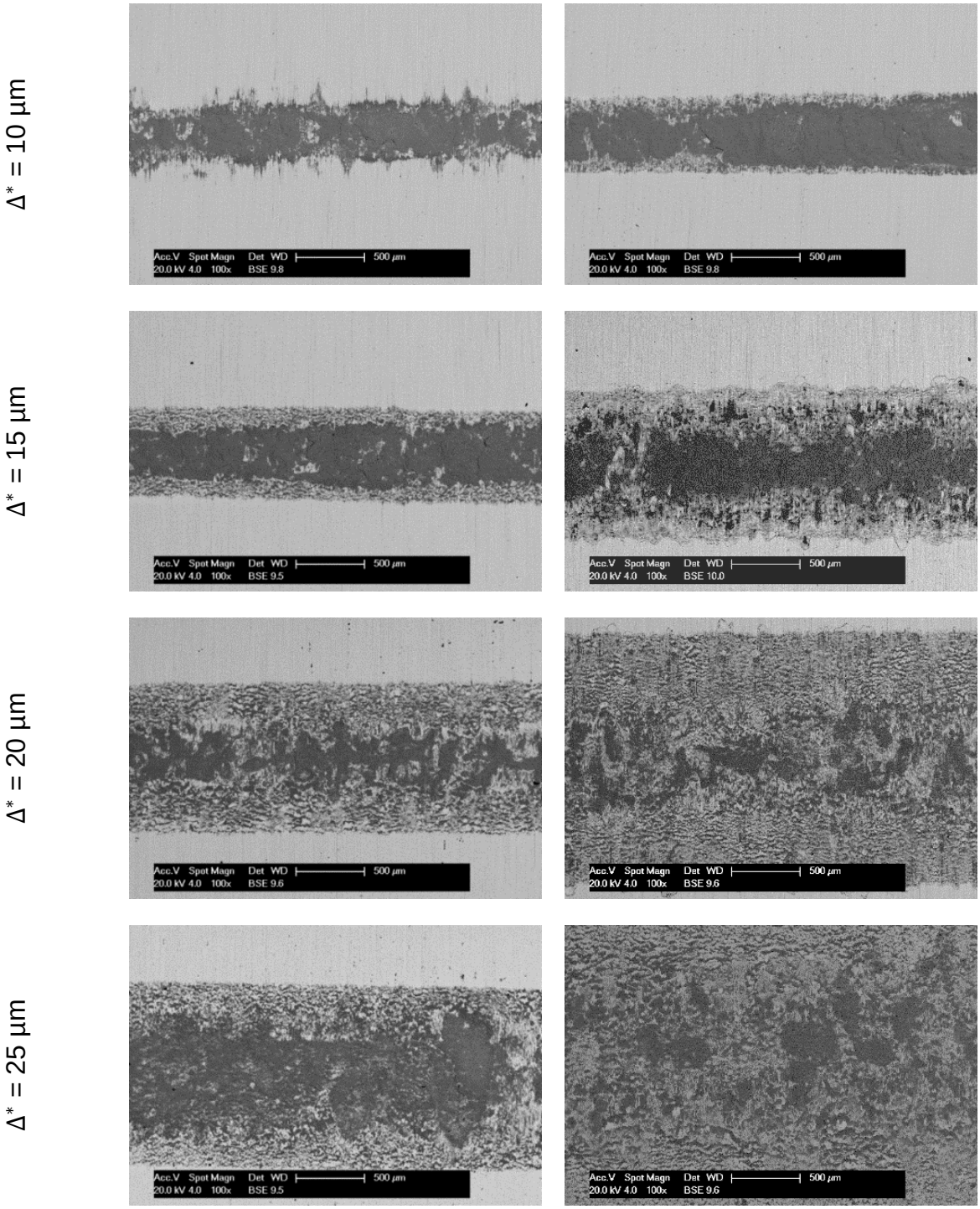

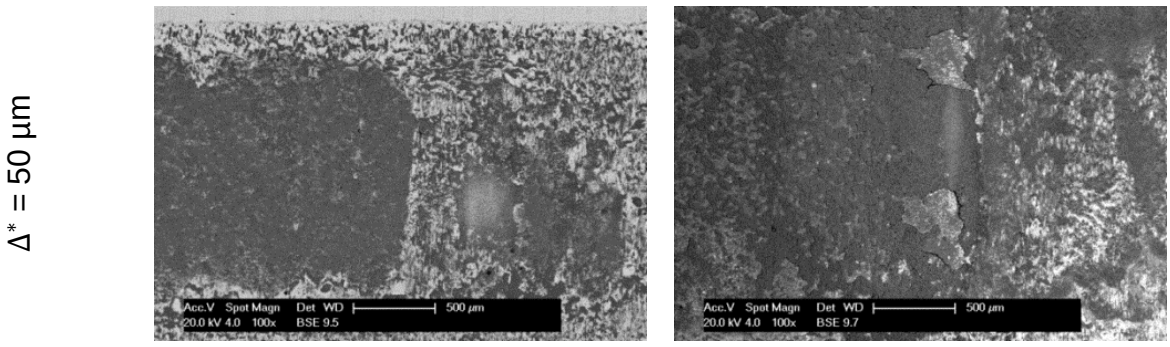

(a) N = 1×10^6 cycles (b) N = 5×10^6 cycles

Figure 9 Low magnification plan-view BSE images of the wear scar on flat specimens for fretting tests at varying displacement amplitudes, from Δ* = 10 µm to Δ* = 50 µm at (a) 1×10^6 cycles; (b) 5×10^6 cycles.

In order to further explore the differences between W-shaped scars and U-shaped scars, the nature of the debris in cross section was also examined, with examples being presented in Figure 10 for tests of duration, N = 5×10^6 cycles at both a low (15 µm) and a high (50 µm) displacement amplitude, Δ*. The low magnification images have a width of ~ 550 µm, whereas the total wear scar widths are 1.2 mm and 3.8 mm for the tests with displacement amplitudes of 15 µm and 50 µm respectively. The scars themselves are very shallow in depth (8 µm and 124 µm for the tests with displacement amplitudes of 15 µm and 50 µm respectively) and at low magnification, it is difficult to discern the overall wear scar shape from the images. However, for scars from tests at both displacement amplitudes, oxide is clearly visible at the wearing surface and appears to be more prevalent in the centre region. At higher magnification, the debris at the centre can be seen to be around 4 – 5 µm in thickness. The profile of the W-shaped wear scar in the case when Δ* = 15 µm shows that the centre region of the W is ~ 9 µm above that of the troughs on either side (see Figure 7b)and thus it can be seen that the bulk of this is the oxide layer itself, which then may provide some protection to the underlying metal; however. The debris layer on the surface of the sample worn with Δ* = 15 µm exhibits a layered structure, but one which is fully oxide in nature (i.e. this material in the centre of the contact is not metallic in nature); in contrast, the debris layer on the surface of the sample worn with Δ* = 50 µm contains fragments of metal (bright) surrounded by an oxide (darker contrast). Given that the debris that emanates from such contacts is largely oxide in nature [9], it is assumed that these metallic fragments will be oxidised as this material travels across the contact on its way to being expelled from the contact.

Δ* = 15 µm Δ* = 50 µm

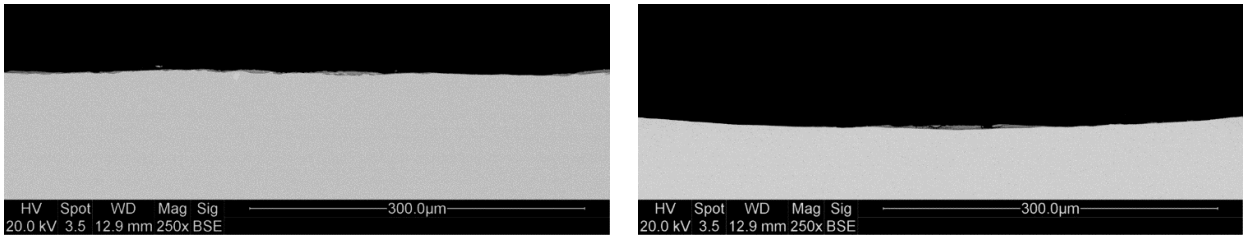

(a) (c)

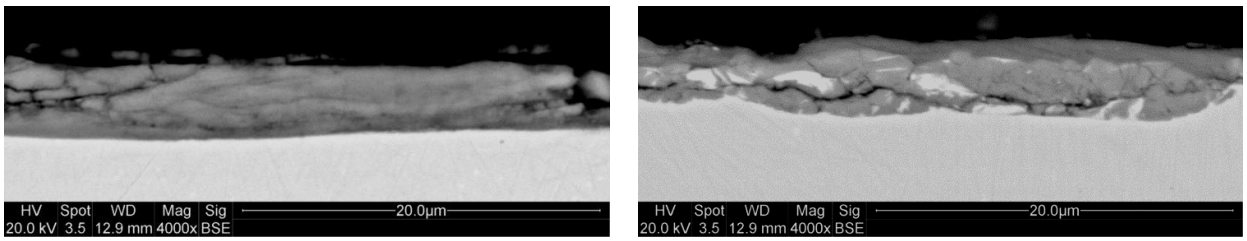

(b) (d)

Figure 10 Cross-sectional micrographs at two magnifications through the centre of wear scars (parallel to the fretting direction) following tests with N = 5×10^6 cycles; (a) and (b) Δ* = 15 µm; (c) and (d) Δ* = 50 µm.

3.5 Determination of the contact size-dependent wear coefficient

Previous work [2] has indicated that the traditional concept of wear rate (Archard-type) fails to give accurate description of fretting wear test when a non-conforming contact geometry is employed, because the wear scar size is constantly changing. A more realistic form of wear equation for the cylinder-on-flat configuration based on the assumption that the debris flow rate should be inversely proportional to the characteristic dimension of wear scar, x, is as presented in Equation 2, with n = 0.75.

As all the specimens in the current study have the same radius (R), the radius in the equation above can be considered as a constant, and therefore Equation 2 can be reduced into a more general form as shown in Equation 4a:

$$V_w = \eta E_d^{0.75} \quad (4a)$$

$$\eta = K R^{-0.25} \quad (4b)$$

$$K = \lambda k^{0.75} \quad (4c)$$

$$V_w = \lambda k^{0.75} R^{-0.25} E_d^{0.75} \quad (4d)$$

where η is the quantity as the product of K and $R^{-0.25}$ (Equation 4b), and as described in the work [2], K is related to the parameter in the governing equation, k, by Equation 4c.

Employing Equation 4a allows Figure 11 to be developed where the ability of Equation 4a to describe wear volume as a sub-linear function of dissipated energy is further demonstrated. Similarly to the work previously reported [2], linear functions can be used to well describe the relationship between the wear volume (V_w) and $E_d^{0.75}$ for different values of Δ* with the coefficient of determination, R^2, being generally high, ranging from $\mathrm{R}^2 = 0.93$ to $\mathrm{R}^2 = 0.99$, with the lower values being observed for the series of tests with Δ* = 10 µm and Δ* = 15 µm. The values of η (and hence K) can, therefore, be determined from Figure 11 as the gradient for each displacement amplitude, Δ*.

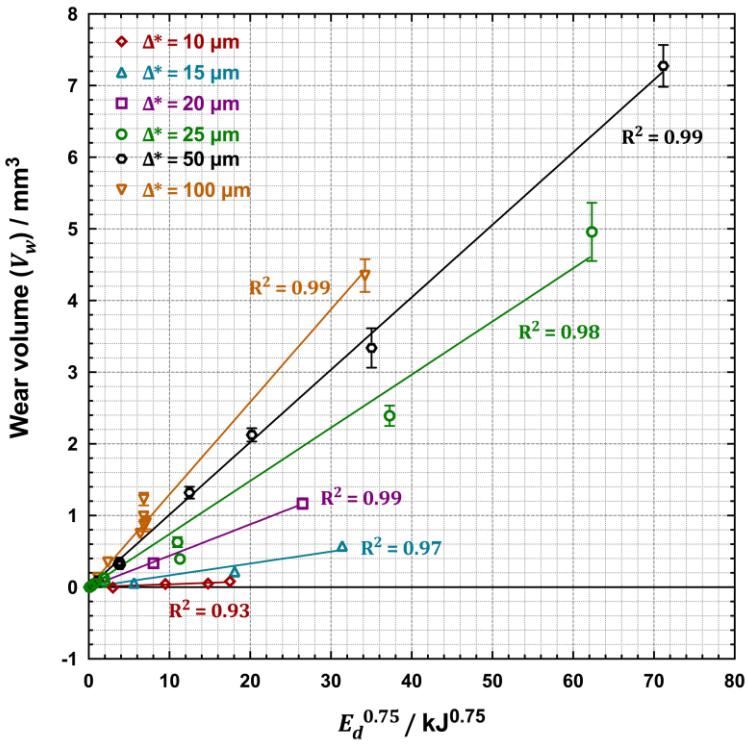

Figure 11 **Plot of wear volume against $E_d^{0.75}$ as suggested by Equation 4a for tests conducted with varying displacement amplitude and number of cycles. It can be seen that η in Equation 4a (indicated by the gradient of the line) is strongly dependent upon displacement amplitude; error bars are displayed.**

With the determination of η and K, values of k can be calculated through Equation 4b and Equation 4c, which are plotted against their corresponding slip amplitude and both presented in Figure 12 and summarised in Table 3; error bars in the graph represent the 95% confidence range of those values. Please note that, although η and K can be easily calculated, it is recognised that the unit of K depends on the choice of contact geometry and the assumption for the governing equation (indicated by Equation 2), and hence lacks a readily apparent physical meaning. In contrast, the parameter k in the governing equation (Equation 2) is easier to explain and understand; thus, further discussion will be focused on k. As can be seen, the dependence of k upon slip amplitude is strongest when the slip amplitude, δ^*, was in the range ~5 μm to ~15 μm (corresponding to displacement amplitudes in the range from Δ^* = 10 μm to Δ^* = 25 μm), whereupon its rate of change decreases with further increase in slip amplitude. One key observation from experimental results is that there seems to exist a correspondence between the changes in μ_e, the changes in the wear scar shape and the changes in k as the displacement amplitude increases; these data are presented together in Table 3.

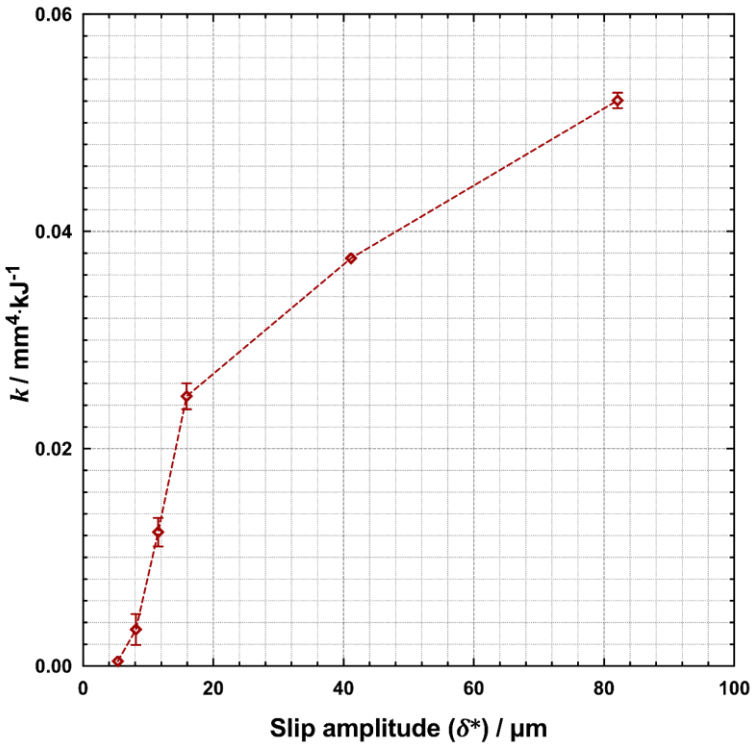

Figure 12 Plot of k as function of slip amplitude.

4 Discussion

4.1 Wear scar characteristics

A small slip amplitude is generally associated with small wear volume if other parameters are fixed, and indeed this is demonstrated by the experimental results presented in this paper. However, it is widely acknowledged that, when the slip amplitude is below a critical value, the process of wear ceases [13, 23, 25, 33] since the debris cannot be readily ejected from the contact. As summarised in Table 3, with the test configuration employed in this work, there are three displacement amplitudes whose equivalent slip amplitude is below or close to 10 μm; namely the cases where Δ^* = 10 μm, Δ^* = 15 μm and Δ^* = 20 μm, with corresponding slip amplitudes of δ^* = 5 μm, δ^* = 8 μm and δ^* = 11 μm. As pointed out by Aldham et al. [16], very long test durations are necessary in fretting to avoid the generation of unrepresentative measurements, and thereby the misinterpretation of data. The threshold slip amplitude is often derived from the measurements where the wear volume is deemed to be negligible, and hence the identification of a threshold may be influenced by the test duration; indeed, this concern is supported by data presented here in Figure 7 and Figure 8. As shown in Figure 7 and Figure 8, when the slip amplitude is beyond the threshold of ~10 μm, a monotonic increase of both the width and depth of wear scars with an increase of slip amplitude is observed. However, it is observed in Figure 7a that, as early as N = 1×10^6 cycles, the wear scar for Δ^* = 20 μm (δ^* = 11 μm) has already developed a wear scar with a wear volume of ~0.34 mm^3 (exhibiting mixed features of W-shaped and U-shaped scars); in contrast, the wear scar for Δ^* = 15 μm (δ^* = 8 μm) is much less developed but still visible (V_w = 0.06 mm^3), whilst the wear scar for Δ^* = 10 μm (δ^* = 5 μm) is almost zero. However, as the test duration is increased to N = 5×10^6 cycles (shown in Figure 7b), the development of wear scars associated with these values of slip amplitude demonstrates a different picture than that observed at N = 1×10^6 cycles: the already developed wear scar for δ^* =

11 μm has grown significantly (V_w = 1.17 mm^3), whilst the wear scar for δ^* = 8 μm starts to show the features of a W-shaped wear scar with a wear volume of 0.22 mm^3; however, there is still very little measurable wear for δ^* = 5 μm. A further increase of test duration to N = 10×10^6 cycles (a test duration rarely seen in literature) as shown in Figure 8 demonstrates that the wear scar for δ^* = 8 μm evolves further with its volume growing to 0.57 mm^3; however, perhaps more significantly, the development of a measurable wear scar for the case of δ^* = 5 μm can finally be observed (V_w = 0.09 mm^3). It is therefore argued here that the evolution of the wear scars for δ^* = 5 μm, δ^* = 8 μm and δ^* = 11 μm under different test durations challenge the current view about the existence of a threshold slip amplitude; it is suggested instead that the initiation of measurable wear may simply take longer as the slip amplitude is reduced.

The low wear volume associated with the small slip amplitude tests may also be explained by the contact being in the partial-slip regime, which is be supported by the fretting loops presented in Figure 4 and the ECoF data presented in Figure 5 and Figure 6. It seems from these figures that the fretting loops are not fully developed for the cases of Δ* = 10 μm and Δ* = 15 μm (δ^* = 5 μm and δ^* = 8 μm respectively), and that their ECoF values are lower than those observed for the higher displacement amplitude tests by ~25%. However, microscopic examination of the surfaces of these wear scars (Figure 9) suggest that there is no evidence of a stuck region on the wear surfaces for either the case of Δ* = 10 μm and Δ* = 15 μm, neither after N = 1×10^6 cycles nor after N = 5×10^6 cycles. In fact, compact debris beds covering those surfaces can be identified; this is in contrast to the wear scar surfaces resulting from fretting tests at the higher slip amplitudes where the coverage of the oxide debris is more sparsely distributed. It is suggested that the low ECoF and the non-fully developed fretting loop for the case of Δ* = 10 μm and Δ* = 15 μm are not caused by the change of regime as suggested by the work of Pearson and Shipway [13]; instead, the variation of debris distribution suggests that the presence of the debris bed acting to fully separate the first bodies is the cause of the reduction in ECoF and the change of shape in the fretting loops.

A higher slip amplitude generally results in a higher power being dissipated into the contact (if fretting frequency is held constant), which is often considered to cause a rise of surface temperature and thereby results in a higher tendency for the debris to sinter [21]. If the surface temperature rise caused by the increase of slip amplitude is a dominating factor, then a more compact debris bed is expected on the contact with larger slip amplitude and a sparser debris bed should be found when the slip amplitude is small. However, this expectation is in contrast to the evidence presented in Figure 9, which is in accord with the observations in wider literature [16, 24, 25]. It is therefore suggested that the effect of any temperature rise caused by the increase of slip amplitude is not a dominating factor.

With the evidence presented in this paper, it is proposed that, when there is no change of fretting regime and when debris ejection remains the RDP, the evolution of wear in fretting follows a similar pattern of development; namely that, similar to the observations in the previous work [6], there is an incubation period for the fretting contact to develop into the steady-state, beyond which the evolution of wear occurs in a manner dictated by the contact geometry. This incubation period is normally characterised by test duration as well as by the threshold energy, and, as already demonstrated by the results in this work, their values are strongly influenced by the test conditions and contact geometries. For example, the test with Δ* = 10 μm (δ^* = 5 μm) requires a very long duration for measurable wear to be initiated, with the incubation period being somewhere between N = 5×10^6 cycles (with E_d = ~20 kJ) and N = 10×10^6 cycles (with E_d = ~45 kJ). The incubation period for the

case of Δ^* = 15 μm (δ^* = 8 μm) is arguably around N = 1×10^6 cycles (E_d = ~10 kJ) where wear can be observed even though its amount is relatively small; for the case of Δ^* = 20 μm (δ^* = 11 μm) and beyond, the incubation period is much shorter; for example, as demonstrated in previous work [6], for δ^* = 41 μm (i.e. Δ^* = 50 μm), the wear scar had already been established by the time when N = 5×10^3 cycles, with E_d = 0.02 kJ. The variation of the incubation period for different slip amplitudes indicates that any attempt to use a unified threshold (either number of cycles or dissipated energy) below which wear will not occur is not appropriate, indicating that the threshold itself is dependent upon the slip amplitude.

To understand the wear behaviour as a function of slip amplitude, it is argued that a sufficient test duration is required to ensure that steady state wear has been reached. To demonstrate the necessity of applying long test durations, Figure 11 has been reproduced (shown in Figure 13) with data associated with two sets of different test durations, each set characterised by a dashed line. It can be seen from Figure 13 that experimental results conducted under the same test duration can be readily fitted with a straight line. Such interpretation of data is commonly seen across a large body of literature [13, 25, 33], which can falsely lead to the concept of threshold. For example, if the investigation was carried out at N = 1×10^6 cycles, then an energy threshold of E_d = ~10 kJ may be reported; but a different value of energy threshold can be found if the individual test duration is extended to N = 5×10^6 cycles. Moreover, as the test duration increases, the so-called “threshold of slip amplitude” will reduce its value continuously, until the slip amplitude is so small that the contact falls into the partial slip regime.

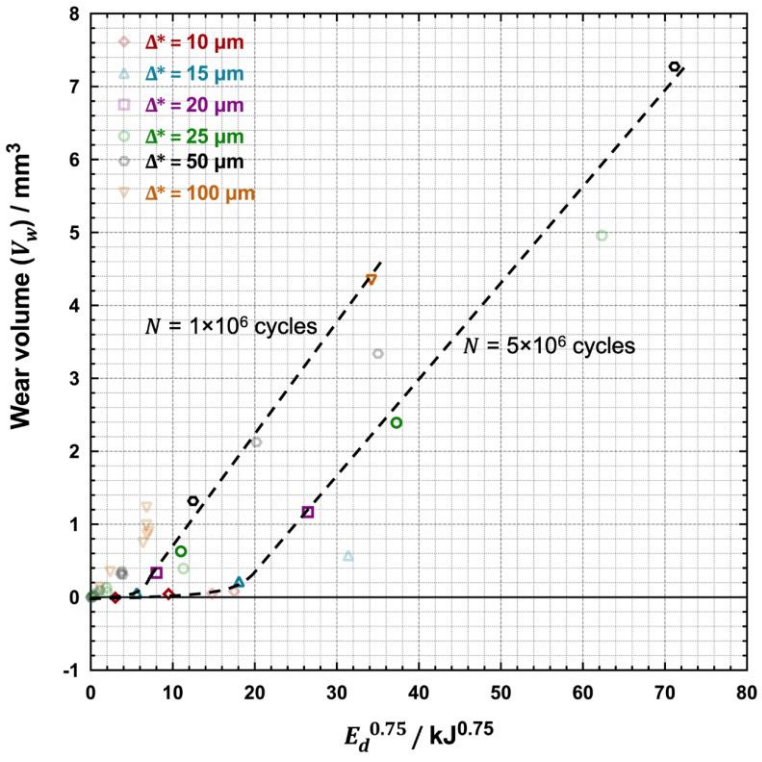

Figure 13 Illustration of the common practice to fit experimental data with straight lines where test durations are fixed by reproducing Figure 11 with original data displayed with a higher transparency; $E_d^{0.75}$ is used as the exposure to wear for the purpose of demonstration.

4.2 Wear rate dependence on slip amplitude in fretting

A demonstrably sufficiently long test duration is suggested as essential when conducting fretting studies. The complete definition of wear incorporates both the process of debris formation and ejection as postulated by the third body approach [4] and the concept of tribology circuit [5]. In this work, it is suggested that, if the debris ejection is the RDP with a cylinder-on-flat contact geometry, the instantaneous wear rate is inversely proportional to the contact size by a parameter k and relationship between the wear volume and the dissipated energy can be described by a non-linear equation as outlined in Equation 2. Whilst it is considered that the larger slip amplitude enhances the rate of debris ejection [16, 17, 24], such an enhancement is competing against the opposite effect brought about by the more rapidly increasing contact size due to the large slip amplitude. To separate the roles of slip amplitude from that of the contact size on debris ejection, the values of K for each slip amplitude can be determined from Figure 11, which is used to calculate their corresponding values of k as presented in Figure 12. As suggested in a previous study [6], the value of k can be interpreted as the ability of the fretting contact to eject oxide debris, and is found to be strongly dependent upon the slip amplitude as indicated by Figure 12. It is recognised that the physical meaning of k is very different from the Archard-type wear rate. Nevertheless, the evolution of k with the increased slip amplitude exhibits a similar pattern which has been observed by those investigations seeking to understand the dependence of Archard-type wear rate upon the slip amplitude [14, 17, 19, 25, 27-29, 33-35].

Figure 12 indicates that the increase of the slip amplitude does indeed result in more efficient debris ejection (i.e. the assumption made in previous work [12] that $\left(\frac{dV}{d\mathrm{N}}\right) \propto \delta^*$ has no validity). The reduced debris ejection rate associated with small slip amplitude will result in a longer debris residence time within the contact, and a higher likelihood of debris agglomeration / sintering to form a compact debris bed. Even though increasing the slip amplitude can enhance the debris ejection, the debris at the centre of wear scar is still more difficult to remove, which may cause the compact debris bed being formed mainly at the centre if it is not able to cover the whole contact (as shown in Figure 9); such a change in the distribution of oxide debris is reflected in the change of k. The development of k also implies that the ability of the motion to remove debris from the contact may approach a plateau since the rate of change of k falls with increasing slip amplitude. If it is assumed that (in the same vein as the proposal of Vingsbo and Söderberg [14]) k will reach a plateau value (above which it is independent of slip amplitude), then such a plateau value has not been reached at least by δ^* = 82 μm. More tests with larger slip amplitudes are required to reveal the evolution of k with values of δ^* greater than 82 μm; equally importantly, more investigations of the dependence of k at higher slip amplitudes are required to understand the underlying physical mechanisms of wear.

The main observation from Figure 7 and Figure 8 is that the shape of wear scar is influenced by the slip amplitude: with the fixed test durations, a W-shaped wear scar is associated with smaller slip amplitudes and U-shaped wear scar can be found with larger slip amplitudes, which is in accord with observations in literature [10, 19, 28, 29]. It is demonstrated in Figure 8c that, with the increase of test duration (as well as energy dissipated) from N = 1×10^6 cycles to N = 5×10^6 cycles, the wear scar for δ^* = 16 μm (Δ^* = 25 μm) changes from U-shaped to W-shaped; it is proposed that this change in shape results from the increase in the wear scar width which accompanies the increase in wear volume as a result of the increased test duration since the increased wear scar width makes debris ejection more difficult leading to the formation of the W-shaped scar. It is proposed here that,

whilst an increase in slip amplitude can promote more efficient debris ejection, this effect is reduced when non-conforming contact geometries are employed by the effect of a more rapidly growing contact size which promotes the formation of W-shaped wear scars. The implication from Figure 8c is that, with the ability to transport debris out the contact defined by a certain slip amplitude, all wear scars in tests with non-conforming geometries may eventually develop into W-shaped wear scars as the contact size increases with test duration; moreover, the contact size at which the transition to a W-shaped scar occurs will increase with increasing slip amplitude.

5 Conclusions

Reducing the slip amplitude leads to the formation of a more compact debris bed across the contact, which is associated with reduced debris ejection and hence the increased residence time for debris inside the contact. As such, reduced ECoF and less developed fretting loops are observed for test conducted with small slip amplitudes. In tests with non-conforming contacts, the enhancement of debris ejection by the increase of slip amplitude is competing against the opposite effect associated with increases in the contact size; the governing equation for the instantaneous wear rate [6] along with the general wear equation in a non-linear form [2] can be used together to separate the effect of the slip amplitude from the effect of the contact size. However, the standard of "long test duration" to reveal the development of wear is influenced by the test conditions. In this paper, it has been shown that the test duration required for wear to begin is increased by the reduction of slip amplitude; under the conditions employed here, a test duration in the order of tens of millions of cycles is needed for tests with δ^* = 5 μm cycles to begin to exhibit the volume loss associated with wear.

For non-conforming contacts, the value of k, the parameter describing the instantaneous wear rate, which is independent of the contact size, can be determined from the transformed experimental data by plotting the wear volume against the quantity of E_d^n (where n = 0.75 if a cylinder-on-flat configuration is employed). The parameter k, which was found to be independent of the contact geometry (as demonstrated in [6]), has been shown to be strongly dependent upon the slip amplitude. Whilst the methods outlined in this paper provide a first attempt to understand the dependence of wear rate on slip amplitude without the effect of contact size, the nature of the change of k in terms of slip amplitude requires further investigation. It is noted that use of conforming contacts in fretting tests (where the contact size does not change as the test proceeds) will significantly simplify the situation, and is recommended for future work examining the dependence of the various processes associated with debris formation and debris ejection upon slip amplitude, although it is noted that contacts of various physical dimension will be required to allow general conclusions to be reached.

6 Funding statement

TZ was a PhD student at the University of Nottingham and his work and studentship were funded by the University of Nottingham.

7 Declaration of competing interest

The authors declare that they have no known competing financial interests or personal relationships that could have appeared to influence the work reported in this paper.

8 Acknowledgements

The authors thank the University of Nottingham for both financial and facility support.

9 References

[1] J.F. Archard, Contact and rubbing of flat surfaces, J Appl Phys, 24 (1953) 981-988.

[2] T. Zhu, P.H. Shipway, Contact size and debris ejection in fretting: The inappropriate use of Archard-type analysis of wear data and the development of alternative wear equations for commonly employed non-conforming specimen pair geometries, Wear, 474-475 (2021) art. no. 203710.

[3] S. Fouvry, P. Kapsa, H. Zahouani, L. Vincent, Wear analysis in fretting of hard coatings throught a dissipated energy concept, Wear, 203-204 (1997) 393-403.

[4] M. Godet, The third-body approach: A mechanical view of wear, Wear, 100 (1984) 437-452.

[5] Y. Berthier, Experimental evidence for friction and wear modelling, Wear, 139 (1990) 77-92.

[6] T. Zhu, P.H. Shipway, W. Sun, The dependence of wear rate on wear scar size in fretting; the role of debris (third body) expulsion from the contact, Wear, 440 (2019) art. no. 203081.

[7] C. Mary, S. Fouvry, J. Martin, B. Bonnet, Pressure and temperature effects on Fretting Wear damage of a Cu–Ni–In plasma coating versus Ti17 titanium alloy contact, Wear, 272 (2011) 18-37.

[8] C. Mary, T. Le Mogne, B. Beaugiraud, B. Vacher, J.M. Martin, S. Fouvry, Tribochemistry of a Ti Alloy Under Fretting in Air: Evidence of Titanium Nitride Formation, Tribology Letters, 34 (2009) 211-222.

[9] A.M. Kirk, W. Sun, C.J. Bennett, P.H. Shipway, Interaction of displacement amplitude and frequency effects in fretting wear of a high strength steel: Impact on debris bed formation and subsurface damage, Wear, 482-483 (2021) art. no. 203981.

[10] S. Fouvry, P. Arnaud, A. Mignot, P. Neubauer, Contact size, frequency and cyclic normal force effects on Ti–6Al–4V fretting wear processes: An approach combining friction power and contact oxygenation, Tribology International, 113 (2017) 460-473.

[11] S. Baydoun, P. Arnaud, S. Fouvry, Modelling adhesive wear extension in fretting interfaces: An advection-dispersion-reaction contact oxygenation approach, Tribology International, 151 (2020) art. no. 106490.

[12] P.H. Shipway, A.M. Kirk, C.J. Bennett, T. Zhu, Understanding and modelling wear rates and mechanisms in fretting via the concept of rate-determining processes - Contact oxygenation, debris formation and debris ejection, Wear, 486-487 (2021) art. no. 204066.

[13] S.R. Pearson, P.H. Shipway, Is the wear coefficient dependent upon slip amplitude in fretting? Vingsbo and Söderberg revisited, Wear, 330 - 331 (2015) 93 - 102.

[14] O. Vingsbo, S. Söderberg, On fretting maps, Wear, 126 (1988) 131-147.

[15] I. Hutchings, P. Shipway, Tribology: Friction and Wear of Engineering Materials, Elsevier Science, 2017.

[16] D. Aldham, J. Warburton, R.E. Pendlebury, The unlubricated fretting wear of mild steel in air, Wear, 106 (1985) 177-201.

[17] S. Fouvry, P. Duó, P. Perruchaut, A quantitative approach of Ti–6Al–4V fretting damage: friction, wear and crack nucleation, Wear, 257 (2004) 916-929.

[18] P.H. Shipway, Time-dependence and exposure-dependence of material removal rates in fretting, Wear, 477 (2021) 203826.

[19] S. Fouvry, P. Kapsa, L. Vincent, Quantification of fretting damage, Wear, 200 (1996) 186-205.

[20] A.R. Warmuth, S.R. Pearson, P.H. Shipway, W. Sun, The effect of contact geometry on fretting wear rates and mechanism for a high strength steel, Wear, 301 (2013) 491 - 500.

[21] X. Jin, P.H. Shipway, W. Sun, The role of frictional power dissipation (as a function of frequency) and test temperature on contact temperature and the subsequent wear behaviour in a stainless steel contact in fretting, Wear, 330-331 (2015) 103-111.

[22] A.R. Warmuth, P.H. Shipway, W. Sun, Fretting wear mapping: The influence of contact geometry and frequency on debris formation and ejection for a steel-on-steel pair, Proceedings of the Royal Society A: Mathematical, Physical and Engineering Science, 471 (2015) art. no. 20140291.

[23] S. Heredia, S. Fouvry, Introduction of a new sliding regime criterion to quantify partial, mixed and gross slip fretting regimes: Correlation with wear and cracking processes, Wear, 269 (2010) 515-524.

[24] J. Warburton, The fretting of mild steel in air, Wear, 131 (1989) 365-386.

[25] N. Ohmae, T. Tsukizoe, The effect of slip amplitude on fretting, Wear, 27 (1974) 281-294.

[26] E.K. Hayes, P.H. Shipway, Effect of test conditions on the temperature at which a protective debris bed is formed in fretting of a high strength steel, Wear, 376 - 377 (2017) 1460 - 1466.

[27] S. Fouvry, C. Poulins, S. Deyber, Impact of contact size and complex gross–partial slip conditions on Ti–6Al–4V/ Ti–6Al–4V fretting wear, Tribology International, 42 (2009) 460 - 473.

[28] S. Baydoun, S. Fouvry, S. Descartes, P. Arnaud, Fretting wear rate evolution of a flat-on-flat low alloyed steel contact: A weighted friction energy formulation, Wear, 426 (2019) 676-693.

[29] S. Baydoun, S. Fouvry, An experimental investigation of adhesive wear extension in fretting interface: Application of the contact oxygenation concept, Tribology International, 147 (2020) art. no. 106266.

[30] A.L. Mohd Tobi, J. Ding, S. Pearson, S.B. Leen, P.H. Shipway, The effect of gross sliding fretting wear on stress distributions in thin W-DLC coating systems, Tribology International, 43 (2010) 1917-1932.

[31] S. Fouvry, P. Kapsa, T. Liskiewicz, S. Hannel, E. Sauger, An energy description of wear mechanisms and its applicatons to oscillation sliding contacts, Wear, 255 (2003) 287 - 298.

[32] X. Jin, W. Sun, P.H. Shipway, Derivation of a wear scar geometry-independent coefficient of friction from fretting loops exhibiting non-Coulomb frictional behaviour, Tribology International, 102 (2016) 561-568.

[33] X.S. Zhang, C.H. Zhange, C.L. Zhu, Slip amplitude effects and microstructural characteristics of surface layers in fretting wear of carbon steel, Wear, 134 (1989) 297-309.

[34] J.S. Halliday, W. Hirst, The fretting corrosion of mild steel, Proceedings of the Royal Society of London. Series A. Mathematical, Physical and Engineering Sciences, 236 (1956) 411-425.

[35] A. Fantetti, L.R. Tamatam, M. Volvert, I. Lawal, L. Liu, L. Salles, M.R.W. Brake, C.W. Schwingshackl, D. Nowell, The impact of fretting wear on structural dynamics: Experiment and Simulation, Tribology International, 138 (2019) 111-124.